Self-consistent force scheme in the spectral multiple-relaxation-time lattice Boltzmann model

Xuhui Li (李旭晖),[1,*] Zuoxu Li (李作旭),[2,†] Wenyang Duan (段文洋),[1,‡] and Xiaowen Shan (单肖文)[3,§]

[1]*College of ShipBuilding Engineering, Harbin Engineering University, Harbin, Heilongjiang 150001, China*

[2]*Department of Mechanics and Aerospace Engineering, Southern University of Science and Technology, Shenzhen, Guangdong 518055, China*

[3]*BNU-HKBU United International College, Zhuhai, Guangdong 519087, China*

(Received 7 December 2022; accepted 19 November 2023; published 10 January 2024)

In the present work, the force term is first derived in the spectral multiple-relaxation-time high-order lattice Boltzmann model. The force term in the Boltzmann equation is expanded in the Hermite temperature rescaled central moment space (RCM), instead of the Hermite raw moment space (RM). The contribution of nonequilibrium RCM moments beyond second order are neglected. For the collision operator in the RCM space, each order of the force term can be incorporated directly. Through the transformation between the RCM space and the RM space, the force term for practical numerical implementation in the RM space can be derived. It can be demonstrated that the present force scheme is self-consistent for the isothermal flow and compressible thermal flow with adjustable Prandtl number via the numerical experiments.

DOI: 10.1103/PhysRevE.109.015301

I. INTRODUCTION

Since the early development of the lattice Boltzmann method (LBM), implementation of the body force term has been generating continued interest [1]. This is especially true in recent years as more complex collision models are adopted in place of the Bhatnagar-Gross-Krook (BGK) [2] model and LBM applied to multiphase flows where the interaction is modeled by a Vlasov body force [3,4]. Both trends call for more accurate treatment of the body force term. Literally a dozen force schemes have been proposed and extensive numerical evaluations conducted [5,6]. Nevertheless, a conclusion has not been reached on how the force term should be implemented independent of the details of the collision model and underlying lattice.

One of the earliest force schemes is the intuitive velocity-shift method used in the modeling of intermolecular interactions [3]. This method shifts the velocity in the equilibrium distribution by $\boldsymbol{g}\Delta t$, where $\boldsymbol{g}$ is the acceleration and Δt the time step. A more refined scheme [7] eliminated the discrete lattice effect by introducing unknown coefficients in the force term and determining them by matching the recovered macroscopic equation with Navier-Stokes equations. Benchmarks in the context of nonideal gas showed that, with the velocity-shift scheme, the equilibrium densities have an unphysical dependence on the relaxation time, whereas with the scheme developed by Yu *et al.* [8] this abnormality is completely eliminated. Li *et al.* [9] analyzed the exact difference method (EDM) [10] and found that its great stability in the Shan-Chen (SC) model [3] is attributed to the extra error introduced to the pressure tensor. Furthermore, Li *et al.* [9] proposed an improved force scheme to deal with the high-density ratio in the SC model. Several force schemes for the central-moment multiple-relaxation-time collision models with standard lattice have also been developed [11–13].

It is worth noting that, in terms of the hydrodynamic moments, the leading effect of all the models are unanimously the same, namely, when considered as an addition to the normal collision term, the zeroth moment of the body force term vanishes to ensure mass conservation and the first moment equals to $\boldsymbol{g}\Delta t$. The subtle differences are only in the second and higher moments representing the additional momentum and energy fluxes caused by the body force. This effect manifests in cases such as multiphase flow modeling where the additional stress plays a significant role [8].

The complexity and controversy are partially due to the fact that the development of the force schemes mostly followed the same *a posteriori* approach of the LB development. The LB equation is constructed as a kinetic model fully discretized in both the velocity and configuration spaces with a discretized time. The errors caused by all discretizations are then optimized to achieve the correct macroscopic Navier-Stokes equation. Besides being disconnected from the Boltzmann equation which includes the effect of the body force, the multiple expansion approach quickly becomes unmanageable for more complex collision models.

In the kinetic theoretical formulation of LB [14,15], the LB equation is obtained by first discretizing the continuum Boltzmann-BGK equation in the velocity space, resulting in a set of partial differential equations for the discretized distribution functions in the velocity space. Without any ambiguity, the body force is given by the finite Hermite expansion of the body force term [15,16]. However, to further discretize it in the temporal and physical space, multiple schemes exist.

The LBE can be obtained by discretizing the discrete-velocity Boltzmann equation in space and time. In presence

*lixuhui@hrbeu.edu.cn
†12032387@mail.sustech.edu.cn
‡duanwenyang@hrbeu.edu.cn
§xiaowenshan@uic.edu.cn

of a body force, the discrete lattice effect can be eliminated [7] *a posteriori*. Actually the same correction can be obtained *a priori* for the BGK model by integrating the discretized Boltzmann equation along the characteristic line together with a trapezoidal rule to handle the collision and body-force terms [17]. The similar approach can be applied to the recently suggested SMRT collision model [18–20] to incorporate the body force.

With the BGK collision model, the description of the collision as a *uniform* relaxation process of the distribution function towards its equilibrium is in many cases simplistic. In a previous series of papers [20–22], the SMRT collision model was developed where the *irreducible components* of the Hermite coefficients are relaxed separately in the reference frame moving with the fluid. These components are the minimum tensor components that can be separately relaxed without violating rotation symmetry.

The rest of the paper is organized as follows. The theoretical derivation is presented in Sec. II with the discrete-velocity force scheme presented in Sec. II A, the derivation of the force scheme for the BGK model in Sec. II B, and the force scheme for the SMRT collision model in Sec. II C. Some numerical verification is given in Sec. III and the conclusion and discussions are given in Sec. IV.

II. BOLTZMANN-BGK EQUATION

A. Background

In kinetic theory [23], the evolution of the single-particle distribution, $f(\boldsymbol{x}, \boldsymbol{\xi}, t)$, under an external or self-generated body force with acceleration $\boldsymbol{g}$ is described by the Boltzmann equation:

$$\frac{\partial f}{\partial t} + \boldsymbol{\xi} \cdot \nabla f + \boldsymbol{g} \cdot \nabla_{\xi} f = \Omega(f), \tag{1}$$

where $\boldsymbol{x}$ and $\boldsymbol{\xi}$ are coordinates in physical and velocity spaces, respectively, t the time, and $\Omega(f)$ the collision term describing the effect of interparticle collision. Due to its extreme complexity, the collision term is often simplified by models, of which the most widely used is the BGK model:

$$\Omega_{\mathrm{BGK}}(f) = -\frac{1}{\tau}\left[f - f^{(eq)}\right], \tag{2}$$

where τ is a relaxation time and $f^{(eq)}$ the Maxwell-Boltzmann distribution. Choosing the characteristic speed $\sqrt{k_B T_0/m_0}$ with k_B the Boltzmann constant and T_0 and m_0 the reference temperature and molecule mass, $f^{(eq)}$ has the dimensionless form

$$f^{(eq)}(\boldsymbol{x}, \boldsymbol{\xi}, t) = \frac{\rho}{(2\pi\theta)^{D/2}} \exp\left[-\frac{(\boldsymbol{\xi} - \boldsymbol{u})^2}{2\theta}\right], \tag{3}$$

where ρ is the density, $\boldsymbol{u}$ the fluid velocity, and $\theta \equiv T/T_0$ the temperature, all dimensionless.

The lattice Boltzmann equation was formulated as a special velocity-space discretization of the Boltzmann equation based on two observations [15]. First, in Chapman-Enskog calculation [24], the macroscopic hydrodynamics only depends on the leading moments of the distribution function rather than its entirety. The distribution function can therefore be approximated by its low-order Hermite expansion without altering the hydrodynamics [25,26]. This truncation is equivalent to projecting Eq. (1) into a low-order Hilbert space spanned by the Hermite polynomials. We denote the Nth order Hermite series by

$$f_N(\boldsymbol{x}, \boldsymbol{\xi}, t) = \omega(\boldsymbol{\xi}) \sum_{n=0}^{N} \frac{1}{n!} \boldsymbol{a}^{(n)} : \mathscr{H}^{(n)}(\boldsymbol{\xi}), \tag{4}$$

where $\mathscr{H}^{(n)}(\boldsymbol{\xi})$ is the nth Hermite polynomial and

$$\omega(\boldsymbol{\xi}) \equiv (2\pi)^{-D/2} \exp(-\xi^2/2) \tag{5}$$

is the weight function with respect to which the Hermite polynomials are orthogonal. The expansion coefficients,

$$\boldsymbol{a}^{(n)}(\boldsymbol{x}, t) = \int f_N(\boldsymbol{x}, \boldsymbol{\xi}, t) \mathscr{H}^{(n)}(\boldsymbol{\xi}) d\boldsymbol{\xi}, \tag{6}$$

are *velocity moments* of the distribution function with the leading few being the familiar hydrodynamic variables, ρ, $\boldsymbol{u}$, and θ.

Second, any finite Hermite series is completely determined by its values on a finite set of $\boldsymbol{\xi}_i$. Let $\{(w_i, \boldsymbol{\xi}_i), i = 1, \ldots, d\}$ be the weights and abscissas of a Qth degree Hermite quadrature such that for any Qth degree polynomial, $p(\boldsymbol{\xi})$, we have

$$\int \omega(\boldsymbol{\xi}) p(\boldsymbol{\xi}) d\boldsymbol{\xi} = \sum_{i=0}^{d} w_i p(\boldsymbol{\xi}_i). \tag{7}$$

The Mth moment of f_N is then

$$\begin{aligned} \int f_N(\boldsymbol{\xi}) \boldsymbol{\xi}^M d\boldsymbol{\xi} &= \int \omega(\boldsymbol{\xi}) \left[\frac{f_N(\boldsymbol{\xi}) \boldsymbol{\xi}^M}{\omega(\boldsymbol{\xi})}\right] d\boldsymbol{\xi} \\ &= \sum_{i=0}^{d} \frac{w_i f_N(\boldsymbol{\xi}_i) \boldsymbol{\xi}_i^M}{\omega(\boldsymbol{\xi}_i)}, \end{aligned} \tag{8}$$

provided that $Q \geqslant M + N$, as the integrand in the brackets is a polynomial of degree $M + N$. Hence all expansion coefficients are completely determined by $f_N(\boldsymbol{\xi}_i)$ as long as $\{\boldsymbol{\xi}_i\}$ forms the abscissas of a quadrature rule of a degree $Q \geqslant 2N$. If we further define the convenience variable

$$f_i \equiv \frac{w_i f_N(\boldsymbol{x}, \boldsymbol{\xi}_i, t)}{\omega(\boldsymbol{\xi}_i)}, \tag{9}$$

the integral velocity moment has the discrete form

$$\int f_N(\boldsymbol{\xi}) \boldsymbol{\xi}^M d\boldsymbol{\xi} = \sum_{i=0}^{d} f_i \boldsymbol{\xi}_i^M, \tag{10}$$

provided that the quadrature conditions are met. Noting by Eq. (6) that the expansion coefficients are also velocity moments, $\boldsymbol{a}^{(n)}$ and f_i can be transformed through the following general discrete Fourier transform:

$$\boldsymbol{a}^{(n)} = \sum_{i=0}^{d} f_i \mathscr{H}^{(n)}(\boldsymbol{\xi}_i), \tag{11a}$$

$$f_i = w_i \sum_{n=0}^{N} \frac{1}{n!} \boldsymbol{a}^{(n)} : \mathscr{H}^{(n)}(\boldsymbol{\xi}_i). \tag{11b}$$

The dynamic equations of f_i are taken as the direct evaluation of the *projected* Eq. (1) at $\boldsymbol{\xi}_i$. This amounts to expanding

all terms in terms of Hermite polynomials and truncating to a finite order. The expansion of $\nabla_\xi f_N$ can be obtained by taking the velocity-space derivative of Eq. (4) and using the following Rodrigues formula

$$\mathscr{H}^{(n)}(\boldsymbol{\xi}) = \frac{(-1)^n}{\omega(\boldsymbol{\xi})}\nabla_{\boldsymbol{\xi}}^n \omega(\boldsymbol{\xi}) \tag{12}$$

to write

$$\begin{aligned}\nabla_{\boldsymbol{\xi}} f_N &= \sum_{n=0}^{N} \frac{1}{n!}\boldsymbol{a}^{(n)} : \nabla_{\boldsymbol{\xi}}[\omega(\boldsymbol{\xi})\mathscr{H}^{(n)}(\boldsymbol{\xi})] \\ &= -\omega(\boldsymbol{\xi})\sum_{n=0}^{N} \frac{1}{n!}\boldsymbol{a}^{(n)} : \mathscr{H}^{(n+1)}(\boldsymbol{\xi}) \\ &= -\omega(\boldsymbol{\xi})\sum_{n=1}^{N+1} \frac{1}{n!}[n\boldsymbol{a}^{(n-1)}] : \mathscr{H}^{(n)}(\boldsymbol{\xi}).\end{aligned} \tag{13}$$

The body-force term, denoted by $F(\boldsymbol{\xi}) \equiv -\boldsymbol{g}\cdot\nabla_{\boldsymbol{\xi}} f_N$, has thus the following expansion:

$$F(\boldsymbol{\xi}) = \omega(\boldsymbol{\xi})\sum_{n=1}^{N+1} \frac{1}{n!}[n\boldsymbol{g}\boldsymbol{a}^{(n-1)}] : \mathscr{H}^{(n)}(\boldsymbol{\xi}). \tag{14}$$

Denoting the Hermite coefficients of $F(\boldsymbol{\xi})$ by $\boldsymbol{a}_F^{(n)}$, we have

$$\boldsymbol{a}_F^{(0)} = 0, \quad \boldsymbol{a}_F^{(n)} = n\boldsymbol{g}\boldsymbol{a}^{(n-1)}, \quad n \geqslant 1, \tag{15}$$

where $\boldsymbol{g}\boldsymbol{a}^{(n-1)}$ is to be understood as the *symmetric product* between $\boldsymbol{g}$ and $\boldsymbol{a}^{(n-1)}$; e.g., in component form, $\boldsymbol{g}\boldsymbol{a}^{(2)} = (g_\alpha a_{\beta\gamma} + g_\beta a_{\gamma\alpha} + g_\gamma a_{\alpha\beta})/3$.

The explicit expressions for the first several orders of $\boldsymbol{a}_0^{(n)}$ can be found in the literature [15]. Thus we have the expanded force term up to the fourth order:

$$\begin{aligned}F \approx \omega(\boldsymbol{\xi})\rho\Bigg\{ &\underbrace{\boldsymbol{g}\cdot\boldsymbol{\xi}}_{1st} + \underbrace{(\boldsymbol{g}\cdot\boldsymbol{\xi})(\boldsymbol{\xi}\cdot\boldsymbol{u}) - \boldsymbol{g}\cdot\boldsymbol{u}}_{2nd} \\ &+ \underbrace{\frac{1}{6\rho}3\boldsymbol{g}\big[\rho[\boldsymbol{u}^2 + (\theta-1)\boldsymbol{\delta}] + \boldsymbol{a}_1^{(2)}\big] : \mathscr{H}^{(3)}(\boldsymbol{\xi})}_{3rd} \\ &+ \underbrace{\frac{1}{24\rho}4\boldsymbol{g}\big(\boldsymbol{a}_0^{(3)} + \boldsymbol{a}_1^{(3)}\big) : \mathscr{H}^{(4)}(\boldsymbol{\xi})}_{4th}\Bigg\},\end{aligned} \tag{16}$$

where the subscripts 0 and 1 denote the zeroth-order (equilibrium) and first-order Chapman-Enskog approximation.

If the expansion of the force term is truncated to second order, the familiar force term can be obtained:

$$F(\boldsymbol{\xi}) = \rho\omega(\boldsymbol{\xi})[\boldsymbol{g}\cdot(\boldsymbol{\xi}-\boldsymbol{u}) + (\boldsymbol{g}\cdot\boldsymbol{\xi})(\boldsymbol{u}\cdot\boldsymbol{\xi})]. \tag{17}$$

Similar to Eq. (9), defining

$$F_i \equiv \frac{w_i F(\boldsymbol{\xi}_i)}{\omega(\boldsymbol{\xi}_i)}, \tag{18}$$

the discrete-velocity Boltzmann equation with body force is

$$\frac{\partial f_i}{\partial t} + \boldsymbol{\xi}_i\cdot\nabla f_i = \Omega_i + F_i, \quad i = 1,\ldots,d. \tag{19}$$

The above equation was previously given by Martys *et al.* [16] and its relations to the previous models were also analyzed. Naturally the body force term is independent of the collision term and, other than the truncation order, there is no ambiguity.

B. Force in LBGK collision model

The discrete-velocity BGK model can be written as

$$\Omega_i = -\frac{1}{\tau}\big[f_i - f_i^{(eq)}\big], \tag{20}$$

where

$$f_i^{(eq)} = \rho w_i\big\{1 + \boldsymbol{u}\cdot\boldsymbol{\xi} + \tfrac{1}{2}[(\boldsymbol{u}\cdot\boldsymbol{\xi})^2 - u^2]\cdots\big\} \tag{21}$$

is the truncated Hermite expansion of the Maxwellian evaluated at $\boldsymbol{\xi}_i$ [15]. The LBE can be obtained by integrating Eq. (19) along the characteristic line and the trapezoidal rule applied to the collision term and force term on the right-hand side as [17,27,28]

$$\begin{aligned}&f_i(\boldsymbol{x}+\boldsymbol{\xi}, t+1) - f_i(\boldsymbol{x}, t) \\ &\quad= \tfrac{1}{2}[\Omega_i(\boldsymbol{x}+\boldsymbol{\xi}, t+1) + \Omega_i(\boldsymbol{x}, t)] \\ &\qquad+ \tfrac{1}{2}[F_i(\boldsymbol{x}+\boldsymbol{\xi}, t+1) + F_i(\boldsymbol{x}, t)],\end{aligned} \tag{22}$$

in which the time step $\Delta t = 1$ is applied for brevity.

We define a new distribution function

$$\bar{f}_i = f_i - \tfrac{1}{2}\Omega_i - \tfrac{1}{2}F_i. \tag{23}$$

Applying the new defined distribution function, the implicit evolution equation (22) can be reconstructed as an explicit evolution equation:

$$\bar{f}_i(\boldsymbol{x}+\boldsymbol{\xi}, t+1) = \bar{f}_i(\boldsymbol{x}, t) + \Omega_i(\boldsymbol{x}, t) + F_i(\boldsymbol{x}, t). \tag{24}$$

Substituting the BGK collision term, Eq. (20), into the above equation and replacing f by $\bar{f}$, $f^{(eq)}$and F_i with Eq. (23), the above evolution equation can be rewritten as the following complete explicit form:

$$\begin{aligned}\bar{f}_i(\boldsymbol{x}+\boldsymbol{\xi}_i, t+1) = \bar{f}_i(\boldsymbol{x}, t) &- \frac{1}{\hat{\tau}}\big[\bar{f}_i(\boldsymbol{x}, t) - f_i^{(eq)}(\boldsymbol{x}, t)\big] \\ &+ \left(1 - \frac{1}{2\hat{\tau}}\right)F_i(\boldsymbol{x}, t),\end{aligned} \tag{25}$$

with $\hat{\tau} = \tau + \frac{1}{2}$. It should be noted that the equilibrium and force term in the above equation are the original forms and $\bar{f}_i$ is the actual distribution function in the numerical implementation.

The zero-order, first-order, and second-order moments of the new defined distribution function can be evaluated according to the original one [28]. The zero-order moment is as follows:

$$\sum \bar{f}_i = \sum\left(f_i + \frac{1}{2\tau}f_i^{(1)} - \frac{1}{2}F_i\right) = \sum f_i, \tag{26}$$

in which the zero-order moments of the nonequilibrium and force term are null. Thus we have

$$\bar{\rho} = \rho. \tag{27}$$

The first-order moment of the new distribution function is as follows:

$$\sum \bar{f}_i \xi_{i,\alpha} = \sum \left(f_i + \frac{1}{2\tau} f_i^{(1)} - \frac{1}{2} F_i \right) \xi_{i,\alpha} = \sum \left(f_i - \frac{1}{2} F_i \right) \xi_{i,\alpha}, \tag{28}$$

in which the first-order moment of the nonequilibrium is null. Thus we have

$$\rho \bar{\boldsymbol{u}} = \rho \boldsymbol{u} - \frac{\rho \boldsymbol{g}}{2}. \tag{29}$$

Then the physical velocity can be written as

$$\boldsymbol{u} = \bar{\boldsymbol{u}} + \frac{\boldsymbol{g}}{2}. \tag{30}$$

The second-order central moment of the new defined distribution function is as follows:

$$\frac{1}{2} \sum \bar{f}_i c_{i,\alpha} c_{i,\beta} = \frac{1}{2} \sum \left(f_i + \frac{1}{2\tau} f_i^{(1)} - \frac{1}{2} F_i \right) c_{i,\alpha} c_{i,\beta} = \frac{1}{2} \sum \left(f_i + \frac{1}{2\tau} f_i^{(1)} \right) c_{i,\alpha} c_{i,\beta}, \tag{31}$$

in which the second-order raw moment of the force term $\sum F_i \xi_{i,\alpha} \xi_{i,\beta} = F_\alpha u_\beta + F_\beta u_\alpha$ is used.

For the monatomic ideal gas or the polyatomic gas without activated internal freedom in D-dimensional space, the temperature θ is related to the internal energy density $\rho\epsilon$ as

$$\frac{D\rho\theta}{2} = \rho\epsilon = \frac{1}{2} \sum f_i c_{i,\alpha} c_{i,\alpha}. \tag{32}$$

Thus taking the trace of the second-order tensors in Eq. (31), we can obtain the following relation as

$$\frac{D\rho\bar{\theta}}{2} = \frac{D\rho\theta}{2}. \tag{33}$$

In the above derivation, the trace of the second term on the right-hand side of Eq. (31) is null. This indicates that the physical temperature is equal to the contraction of the second-order central moment of the new distribution function

$$\theta = \bar{\theta}. \tag{34}$$

It is worth noting that the macroscopic variables used in the equilibrium and force term in Eq. (25) are the physical variables $\rho, \boldsymbol{u}, \theta$, instead of $\bar{\rho}, \bar{\boldsymbol{u}}, \bar{\theta}$. If thermohydrodynamic level is not considered and the force term is only expanded to second order, it is reduced to the force scheme derived by He *et al.* [17].

C. Force in SMRT collision model

The force scheme in the raw-moment Hermite MRT collision model is organized in the Appendix for the interested readers. We now apply the same technique to derive the space-time discretization for the central-moment based SMRT collision model [18–20]. Briefly, the expansion of Eq. (4) is made in the reference frame moving with fluid. Namely the Hermite polynomials are with respect to $\boldsymbol{v} \equiv (\boldsymbol{\xi} - \boldsymbol{u})/\sqrt{\theta}$ as

$$f_N(\boldsymbol{x}, \boldsymbol{v}, t) = \omega(\boldsymbol{v}) \sum_{n=0}^{N} \frac{1}{n!} \boldsymbol{d}^{(n)} : \mathscr{H}^{(n)}(\boldsymbol{v}), \tag{35}$$

with $\boldsymbol{d}^{(n)}(\boldsymbol{x}, t)$ being the expansion coefficients given by

$$\boldsymbol{d}^{(n)}(\boldsymbol{x}, t) = \int f_N(\boldsymbol{x}, \boldsymbol{v}, t) \mathscr{H}^{(n)}(\boldsymbol{v}) d\boldsymbol{v}. \tag{36}$$

Note that this is precisely the Hermite polynomials used by Grad [26]. The Maxwell-Boltzmann equilibrium distribution is related to the weight function by

$$f^{(0)}(\boldsymbol{v}) = \rho\theta^{-D/2} \omega(\boldsymbol{v}). \tag{37}$$

Its Hermite expansion coefficients, denoted by $\boldsymbol{d}_0^{(n)}$, are hence

$$\boldsymbol{d}_0^{(n)} = \begin{cases} \rho\theta^{-D/2}, & n = 0, \\ 0, & n > 0. \end{cases} \tag{38}$$

Owing to the conservation of mass and momentum, we have $\boldsymbol{d}^{(0)} = \boldsymbol{d}_0^{(0)}$ and $\boldsymbol{d}^{(1)} = \boldsymbol{d}_0^{(1)} = 0$. Similar to Eq. (14), the expansion of the body-force term in the Hermite rescaled central moment (Hermite RCM) space is as follows:

$$F = \frac{\omega(\boldsymbol{v})}{\sqrt{\theta}} \sum_{n=1}^{N} \frac{1}{n!} \left[n\boldsymbol{g} \left(\boldsymbol{d}_0^{(n-1)} + \boldsymbol{d}_1^{(n-1)} \right) \right] : \mathscr{H}^{(n)}(\boldsymbol{v}), \tag{39}$$

in which the relation $\nabla_{\boldsymbol{\xi}} = \frac{1}{\sqrt{\theta}} \nabla_{\boldsymbol{v}}$ is applied and $\boldsymbol{d}_1^{(n)}$ denotes the nonequilibrium Hermite RCM. The detailed expansion form for the first several orders is as follows:

$$F \approx \frac{1}{\sqrt{\theta}} \omega(\boldsymbol{v}) \rho \Bigg\{ \underbrace{\theta^{-D/2} \boldsymbol{g} \cdot \boldsymbol{v}}_{1st} + \underbrace{\frac{1}{2\rho} \theta^{-(D+1)/2} 2 \left(\boldsymbol{g} \frac{-\boldsymbol{F}}{2} \right) : \mathscr{H}^{(2)}(\boldsymbol{\xi})}_{2nd} + \underbrace{\frac{1}{6\rho} \theta^{-(D+2)/2} 3\boldsymbol{g} (\boldsymbol{a}_1^{(2)} + \boldsymbol{u}\boldsymbol{F}) : \mathscr{H}^{(3)}(\boldsymbol{v})}_{3rd} + \underbrace{\frac{1}{24\rho} \theta^{-(D+3)/2} 4\boldsymbol{g} \left(\boldsymbol{a}_1^{(3)} - 3\boldsymbol{u}\boldsymbol{a}_1^{(2)} - \frac{3}{2} \boldsymbol{u}_1 \boldsymbol{F} \right) : \mathscr{H}^{(4)}(\boldsymbol{v})}_{4th} \Bigg\}, \tag{40}$$

in which $\boldsymbol{u}_1 = \boldsymbol{u}^2 - (\theta - 1)\boldsymbol{\delta}$.

For the purpose of convenience, we define the Hermite coefficients of the force term as

$$\boldsymbol{d}_F^{(n)} = \frac{1}{\sqrt{\theta}} n\boldsymbol{g}\boldsymbol{d}^{(n-1)}, \quad n \geqslant 1. \tag{41}$$

In particular, we have $\theta^{(D+1)/2} \boldsymbol{d}_F^{(1)} = \rho\boldsymbol{g}$. Furthermore, if the contributions from the nonequilibrium beyond second order are neglected, we have $\theta^{(D+2)/2} \boldsymbol{d}_F^{(2)} = -\boldsymbol{F}\boldsymbol{g}$, $\theta^{(D+3)/2} \boldsymbol{d}_F^{(3)} = 3\boldsymbol{g}\boldsymbol{u}\boldsymbol{F}$, and $\theta^{(D+4)/2} \boldsymbol{d}_F^{(4)} = -6\boldsymbol{g}\boldsymbol{u}_1\boldsymbol{F}$.

To allow maximum flexibility while preserving rotational symmetry [20–22], each $\mathscr{H}^{(n)}(\boldsymbol{v})$ is further decomposed into its traceless components, $\mathscr{S}^{(n,k)}(\boldsymbol{v})$. Let the distribution function have the following expansions:

$$f(\boldsymbol{v}) = \omega(\boldsymbol{v}) \sum_{n=0}^{N} \frac{1}{n!} \sum_{k} \boldsymbol{d}^{(n,k)} : \mathscr{S}^{(n,k)}(\boldsymbol{v}) \tag{42}$$

and $\boldsymbol{d}_\Omega^{(n,k)}$ the coefficients of the similar expansion of the collision operator which is defined as the independent relaxation

of each traceless component, i.e.,

$$\begin{aligned}\boldsymbol{d}_{\Omega}^{(n,k)} &= -\frac{1}{\tau_{nk}}\left(\boldsymbol{d}^{(n,k)} - \boldsymbol{d}_{0}^{(n,k)}\right)\\ &= -\frac{1}{\tau_{nk}}\boldsymbol{d}^{(n,k)}, \quad n = 1, \ldots, N,\end{aligned} \tag{43}$$

where τ_{nk} are relaxation times.

In the face of this complicated collision operator, the technique of the previous section can still be applied. Equation (11a) indicates the transform from the phase space to the Hermite raw moment (Hermite RM) space. Similarly, we denote the transform from the phase space to the Hermite RCM space, i.e., f_i to $\boldsymbol{d}^{(n,k)}$, as

$$M_{nk}(f_i) = \boldsymbol{d}^{(n,k)}. \tag{44}$$

By Eq. (43), we have

$$M_{nk}(\Omega_i) = -\frac{1}{\tau_{nk}}\boldsymbol{d}^{(n,k)}. \tag{45}$$

The discrete-velocity Boltzmann equation (19) is independent of lattice, collision model, and force term. For any of them, we can get the same evolution equation as Eq. (24), in which the right-hand side stores the information of the present location and time while the left-hand side stores information after the streaming process. The transform of the right-hand side of Eq. (24) to the Hermite RCM space is

$$\bar{\boldsymbol{d}}_{p}^{(n,k)} = \bar{\boldsymbol{d}}^{(n,k)} - \frac{1}{\tau_{nk}}\boldsymbol{d}^{(n,k)} + \boldsymbol{d}_{F}^{(n,k)}, \quad n \geqslant 1, \tag{46}$$

in which the subscript p denotes the postcollision state and $\bar{\boldsymbol{d}}^{(n,k)}$ is the mapping of Eq. (23) in Hermite RCM space

$$\bar{\boldsymbol{d}}^{(n,k)} = \boldsymbol{d}^{(n,k)} + \frac{1}{2\tau_{nk}}\boldsymbol{d}^{(n,k)} - \frac{1}{2}\boldsymbol{d}_{F}^{(n,k)}, \quad n \geqslant 1. \tag{47}$$

Specifically, $\bar{\boldsymbol{d}}^{(1,k)} = -\frac{1}{2}\boldsymbol{d}_{F}^{(1,k)}$.

Thus Eq. (46) can be written as the following explicit form:

$$\bar{\boldsymbol{d}}_{p}^{(n,k)} = \left(1 - \frac{1}{\hat{\tau}_{nk}}\right)\bar{\boldsymbol{d}}_{1}^{(n,k)} + \left(1 - \frac{1}{2\hat{\tau}_{nk}}\right)\boldsymbol{d}_{F}^{(n,k)}, \quad n \geqslant 1, \tag{48}$$

in which $\hat{\tau}_{nk} = \tau_{nk} + \frac{1}{2}$ and $\bar{\boldsymbol{d}}_{1}^{(n,k)} = \bar{\boldsymbol{d}}^{(n,k)} - \boldsymbol{d}_{0}^{(n,k)}$. For $n = 1$, we have $\bar{\boldsymbol{d}}_{p}^{(1)} = \frac{1}{2}\boldsymbol{d}_{F}^{(1)}$.

To avoid the interpolation operation in the stream process, the postcollision Hermite RCMs need to be transferred to the Hermite RM space and then reconstruct the postcollision distribution function. Similar to the relations between the Hermite RCMs and Hermite RMs of nonequilibrium as [19,28], the transformation for the first several orders are as follows:

$$\bar{\boldsymbol{a}}_{p}^{(0)} = 0, \tag{49a}$$

$$\bar{\boldsymbol{a}}_{p}^{(1)} = \theta^{\frac{D+1}{2}}\bar{\boldsymbol{d}}_{p}^{(1)} = \frac{\rho\boldsymbol{g}}{2}, \tag{49b}$$

$$\begin{aligned}\bar{\boldsymbol{a}}_{p}^{(2)} &= \theta^{\frac{D+2}{2}}\left(1 - \frac{1}{\hat{\tau}_{2}}\right)\bar{\boldsymbol{d}}_{1}^{(2)} + 2\boldsymbol{u}\bar{\boldsymbol{a}}_{p}^{(1)} - \left(1 - \frac{1}{2\hat{\tau}_{2}}\right)(\boldsymbol{F}\boldsymbol{g})\\ &= \left(1 - \frac{1}{\hat{\tau}_{2}}\right)\left(\bar{\boldsymbol{a}}_{1}^{(2)} - 2\boldsymbol{u}\bar{\boldsymbol{a}}_{1}^{(1)}\right) + 2\boldsymbol{u}\bar{\boldsymbol{a}}_{p}^{(1)} - \left(1 - \frac{1}{2\hat{\tau}_{2}}\right)(\boldsymbol{F}\boldsymbol{g}),\end{aligned} \tag{49c}$$

$$\begin{aligned}\bar{\boldsymbol{a}}_{p}^{(3)} &= \theta^{\frac{D+3}{2}}\left(1 - \frac{1}{\hat{\tau}_{3}}\right)\bar{\boldsymbol{d}}_{1}^{(3)} + 3\boldsymbol{u}\bar{\boldsymbol{a}}_{p}^{(2)} - 3\boldsymbol{u}_{1}\bar{\boldsymbol{a}}_{p}^{(1)} + \left(1 - \frac{1}{2\hat{\tau}_{3}}\right)(3\boldsymbol{g}\boldsymbol{u}\boldsymbol{F})\\ &= \left(1 - \frac{1}{\hat{\tau}_{3}}\right)\left(\bar{\boldsymbol{a}}_{1}^{(3)} - 3\boldsymbol{u}\bar{\boldsymbol{a}}_{1}^{(2)} + 3\boldsymbol{u}_{1}\bar{\boldsymbol{a}}_{1}^{(1)}\right) + 3\boldsymbol{u}\bar{\boldsymbol{a}}_{p}^{(2)} - 3\boldsymbol{u}_{1}\bar{\boldsymbol{a}}_{p}^{(1)} + \left(1 - \frac{1}{2\hat{\tau}_{3}}\right)(3\boldsymbol{g}\boldsymbol{u}\boldsymbol{F}),\end{aligned} \tag{49d}$$

$$\begin{aligned}\bar{\boldsymbol{a}}_{p}^{(4)} &= \theta^{\frac{D+4}{2}}\left(1 - \frac{1}{\hat{\tau}_{4}}\right)\bar{\boldsymbol{d}}_{1}^{(4)} + 4\boldsymbol{u}\bar{\boldsymbol{a}}_{p}^{(3)} - 6\boldsymbol{u}_{1}\bar{\boldsymbol{a}}_{p}^{(2)} + 4(\boldsymbol{u}\boldsymbol{u}_{2})\bar{\boldsymbol{a}}_{p}^{(1)} + \left(1 - \frac{1}{2\hat{\tau}_{4}}\right)(-6\boldsymbol{g}\boldsymbol{u}_{1}\boldsymbol{F})\\ &= \left(1 - \frac{1}{\hat{\tau}_{4}}\right)\left(\bar{\boldsymbol{a}}_{1}^{(4)} - 4\boldsymbol{u}\bar{\boldsymbol{a}}_{1}^{(3)} + 6\boldsymbol{u}_{1}\bar{\boldsymbol{a}}_{1}^{(2)} - 4\boldsymbol{u}\boldsymbol{u}_{2}\bar{\boldsymbol{a}}_{1}^{(1)}\right) + 4\boldsymbol{u}\bar{\boldsymbol{a}}_{p}^{(3)} - 6\boldsymbol{u}_{1}\bar{\boldsymbol{a}}_{p}^{(2)} + 4\boldsymbol{u}\boldsymbol{u}_{2}\bar{\boldsymbol{a}}_{p}^{(1)} + \left(1 - \frac{1}{2\hat{\tau}_{4}}\right)(-6\boldsymbol{g}\boldsymbol{u}_{1}\boldsymbol{F}),\end{aligned} \tag{49e}$$

in which $\bar{\boldsymbol{a}}_{p}^{(n)}$ denotes the postcollision Hermite RMs except the equilibrium and $\boldsymbol{u}_2 = \boldsymbol{u}^2 - 3(\theta - 1)\boldsymbol{\delta}$. Since the bulk viscosity and the multiple relaxation rates of higher orders are not discussed in the present work, the simplified form of Eq. (48) with one relaxation rate at each order is elaborated in the above equations. The fourth-order collision term $(1 - \frac{1}{\hat{\tau}_4})\bar{\boldsymbol{d}}_{1}^{(4)}$ will be trimmed once $\hat{\tau}_4 = 1$ as the regularization applied in the previous work [19]. The transformations are not limited to the first four orders, but it is sufficient for the NSF hierarchy [19].

If the recursive collision terms of lower orders in the collision terms of higher order are explicitly substituted, then the above collision model can be organized to the following obvious forms with some simple algebraic operations:

$$\bar{\boldsymbol{a}}_p^{(0)} = 0, \tag{50a}$$

$$\bar{\boldsymbol{a}}_p^{(1)} = \frac{\rho \boldsymbol{g}}{2} = \frac{1}{2}\boldsymbol{a}_F^{(1)}, \tag{50b}$$

$$\bar{\boldsymbol{a}}_p^{(2)} = \left(1-\frac{1}{\hat{\tau}_2}\right)\bar{\boldsymbol{a}}_1^{(2)} + \left(1-\frac{1}{2\hat{\tau}_2}\right)\boldsymbol{a}_F^{(2)}, \tag{50c}$$

$$\begin{aligned}\bar{\boldsymbol{a}}_p^{(3)} &= \left(1-\frac{1}{\hat{\tau}_3}\right)\left(\bar{\boldsymbol{a}}_1^{(3)} - 3\boldsymbol{u}\bar{\boldsymbol{a}}_1^{(2)} + 3\boldsymbol{u}_1\bar{\boldsymbol{a}}_1^{(1)}\right) + 3\boldsymbol{u}\bar{\boldsymbol{a}}_p^{(2)} - 3\boldsymbol{u}_1\bar{\boldsymbol{a}}_p^{(1)} + \left(1-\frac{1}{2\hat{\tau}_3}\right)(3\boldsymbol{g}\boldsymbol{u}\boldsymbol{F}) \\ &= \left(1-\frac{1}{\hat{\tau}_3}\right)\bar{\boldsymbol{a}}_1^{(3)} + \left(1-\frac{1}{2\hat{\tau}_3}\right)\boldsymbol{a}_F^{(3)} + \underbrace{\left(\frac{1}{\hat{\tau}_3}-\frac{1}{\hat{\tau}_2}\right)3\boldsymbol{u}\bar{\boldsymbol{a}}_1^{(2)} + \left(\frac{1}{2\hat{\tau}_3}-\frac{1}{2\hat{\tau}_2}\right)3\boldsymbol{u}\boldsymbol{a}_F^{(2)}}, \end{aligned} \tag{50d}$$

$$\begin{aligned}\bar{\boldsymbol{a}}_p^{(4)} &= \left(1-\frac{1}{\hat{\tau}_4}\right)\left(\bar{\boldsymbol{a}}_1^{(4)} - 4\boldsymbol{u}\bar{\boldsymbol{a}}_1^{(3)} + 6\boldsymbol{u}_1\bar{\boldsymbol{a}}_1^{(2)} - 4\boldsymbol{u}\boldsymbol{u}_2\bar{\boldsymbol{a}}_1^{(1)}\right) + 4\boldsymbol{u}\bar{\boldsymbol{a}}_p^{(3)} - 6\boldsymbol{u}_1\bar{\boldsymbol{a}}_p^{(2)} + 4(\boldsymbol{u}\boldsymbol{u}_2)\bar{\boldsymbol{a}}_p^{(1)} + \left(1-\frac{\omega_4}{2}\right)(-6\boldsymbol{g}\boldsymbol{u}_1\boldsymbol{F}) \\ &= \left(1-\frac{1}{\hat{\tau}_4}\right)\bar{\boldsymbol{a}}_1^{(4)} + \left(1-\frac{1}{2\hat{\tau}_4}\right)\boldsymbol{a}_F^{(4)} + \underbrace{\left(\frac{1}{\hat{\tau}_4}-\frac{1}{\hat{\tau}_3}\right)4\boldsymbol{u}\bar{\boldsymbol{a}}_1^{(3)} + \left(\frac{1}{2\hat{\tau}_4}-\frac{1}{2\hat{\tau}_3}\right)4\boldsymbol{u}\boldsymbol{a}_F^{(3)}} \\ &\quad - \underbrace{\left[\left(\frac{1}{\hat{\tau}_2}+\frac{1}{\hat{\tau}_4}-\frac{2}{\hat{\tau}_3}\right)6\boldsymbol{u}\boldsymbol{u} + \left(\frac{1}{\hat{\tau}_2}-\frac{1}{\hat{\tau}_4}\right)6(\theta-1)\boldsymbol{\delta}\right]\bar{\boldsymbol{a}}_1^{(2)}} - \underbrace{\left[\left(\frac{1}{2\hat{\tau}_2}+\frac{1}{2\hat{\tau}_4}-\frac{1}{\hat{\tau}_3}\right)6\boldsymbol{u}\boldsymbol{u} + \left(\frac{1}{2\hat{\tau}_2}-\frac{1}{2\hat{\tau}_4}\right)6(\theta-1)\boldsymbol{\delta}\right]\boldsymbol{a}_F^{(2)}}. \end{aligned} \tag{50e}$$

In the above collision equations, the underbrace part of the third-order collision term will only vanish when $\hat{\tau}_3 = \hat{\tau}_2$, i.e., $\mathrm{Pr} = 1$. The underbrace part of the fourth-order collision term will vanish once $\hat{\tau}_2 = \hat{\tau}_3 = \hat{\tau}_4$, which indicates that the collision process in RM space is identical to those in the RCM space if and only if one relaxation rate is applied. The solutions of $\bar{\boldsymbol{a}}_1^{(n)}$ and $\boldsymbol{a}_F^{(n)}$ can be found in the Appendix. In the numerical implementations, both forms of collision models, Eq. (49) and Eq. (50), can be applied actually.

The postcollision distribution function can be constructed by the Hermite expansion as

$$\bar{f}_{i,p} = \omega_i \sum_{n=0}^{4} \frac{1}{n!}\left(\boldsymbol{a}_0^{(n)} + \bar{\boldsymbol{a}}_p^{(n)}\right) : \mathscr{H}^{(n)}(\boldsymbol{\xi}_i). \tag{51}$$

Then the stream can be conducted as

$$f_i(\boldsymbol{x} + \boldsymbol{\xi}_i, t+1) = \bar{f}_{i,p}(\boldsymbol{x}, t). \tag{52}$$

III. NUMERICAL SIMULATION

In this section, three numerical benchmarks are tested to verify the effectiveness and accuracy of the present force scheme in the SMRT collision model. The lattice applied in these benchmarks is the D2V37a lattice [18]. The first benchmark is the Taylor-Green flow with given force field but without boundary condition treatment, which is performed to verify the convergence order of the present scheme. The second one is the isothermal Womersley flow with boundary condition, which aims to test the accuracy of the present scheme with unsteady force field. The third numerical example is the compressible Poiseuille flow, which is applied to test the accuracy of the present force scheme for the compressible thermal flow with arbitrary Prandtl number.

A. Taylor-Green flow

For the two-dimensional Taylor-Green flow within the periodic domain $[L, L]$, the analytical unsteady force is exerted on the flow field

$$\boldsymbol{F}(x, y) = -\frac{\rho u_0^2}{2}\left[k_1 \sin(2k_1 x), \frac{k_1^2}{k_2}\sin(2k_2 y)\right]e^{t^*}, \tag{53}$$

in which $k_1 = 2\pi/L$, $k_2 = 2\pi/L$, and ν is the kinematic viscosity; $u_0 = 0.002$ is the reference velocity. The flow field has the analytical solution

$$\boldsymbol{u}_a = -u_0\left[\cos(k_1 x)\sin(k_2 y), -\frac{k_1}{k_2}\sin(k_1 x)\cos(k_2 y)\right]e^{t^*}, \tag{54}$$

in which $t^* = -2(k_1^2 + k_2^2)\nu t$. The flow is characterized by the Reynolds number, $\mathrm{Re} = u_0 L/\nu$. In the simulation, the computational domain is resolved by a series of grid nodes, $L = [16, 32, 64, 128, 256, 384]$, with $\mathrm{Re} = 50$. In Fig. 1, the horizontal velocity profile along the vertical center line and the vertical velocity profile along the horizontal center line are depicted. It can be found that the numerical simulation results agree well with the analytical solution at different specific times. Figure 2 depicts the global error with different resolutions in contrast with the analytical solutions. The global error is defined in Eq. (55):

$$E_2 = \sqrt{\frac{\sum(\boldsymbol{u} - \boldsymbol{u}_a)^2}{\sum \boldsymbol{u}_a^2}}. \tag{55}$$

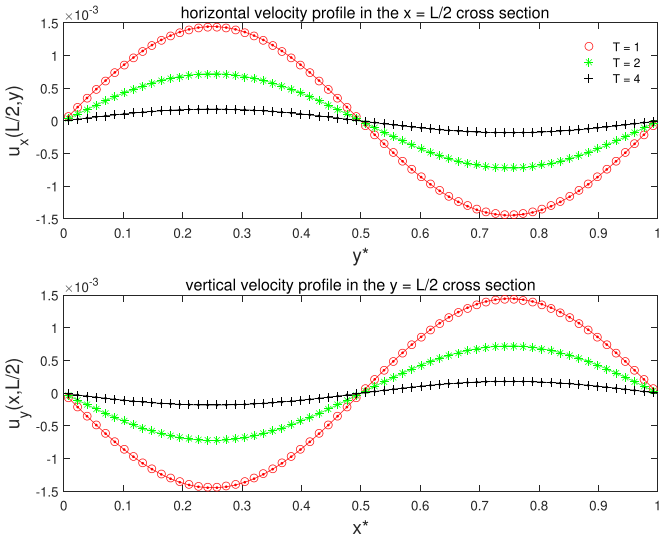

FIG. 1. Numerical (symbols; resolution: 64×64) and analytical (solid line) results of 2D Taylor-Green flow at different times $t = nT$ with $n = 1, 2, 4$ and $T = \ln 2/(2\nu k_1^2)$.

B. Womersley flow

The second numerical benchmark is the Womersley flow. In this numerical case, the flow is bounded by two parallel plates and a periodic pressure gradient or a periodic force is exerted on the flow, which results in an unsteady flow. The periodic force is $Fx(t) = -A_p \cos(\omega t)$, where A_p is the amplitude and $\omega = 2\pi/T$ is the frequency. Obviously, $Fx(t)$ is spatially uniform but temporally unsteady. The analytical solution of the velocity field for the Womersley flow is given by

$$U(y,t) = \mathrm{Re}\left(i\frac{A_p}{\rho_0 \omega}\left\{ 1 - \frac{\cosh\left[(1+i)y\sqrt{\frac{\omega}{2\nu}}\right]}{\cosh\left[(1+i)L\sqrt{\frac{\omega}{2\nu}}\right]}\right\} e^{i\omega t}\right), \quad (56)$$

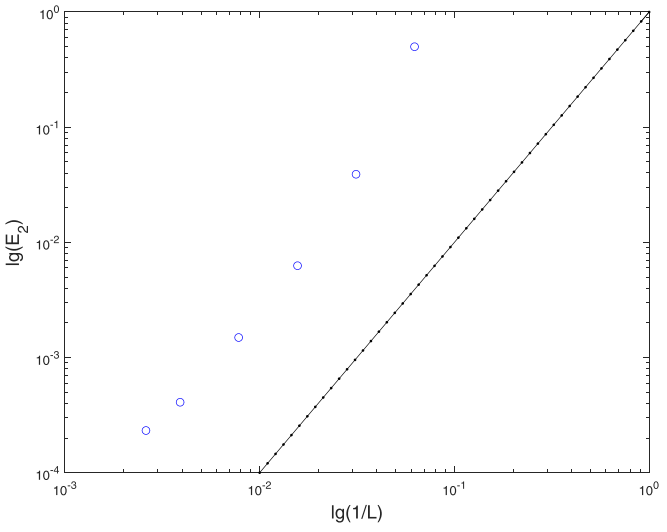

FIG. 2. Convergence test: six resolutions are tested (16×16, 32×32, 64×64, 128×128, 256×256, and 384×384), the solid dot line is of slope 2, and the convergence order of the present numerical results is between first and second order.

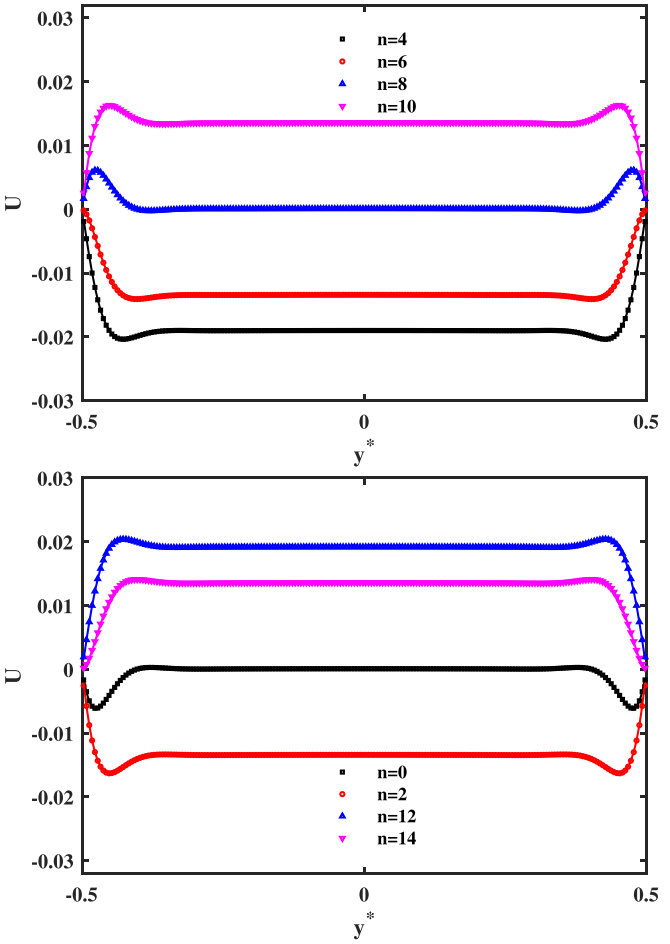

FIG. 3. Numerical (symbols) and analytical (solid line) results of Womersley flow at different times $t = nT/16$ with (a) $n = 4, 6, 8, 10$ and (b) $n = 0, 2, 12, 14$.

where $y \in [-L, L]$, with $2L$ being the channel width, ν is the kinematic viscosity, and Re denotes the real part of the complex number.

The simulations are carried out in a computational domain with $Nx \times Ny = 50 \times 200$. In the x direction, the periodic boundary condition is applied. The diffuse reflection boundary condition [29] is imposed on the two plates. The period T is set as 1200, the kinematic viscosity is chosen as $\nu = 0.1$, and the amplitude Ap is set as 0.0001. The initial density is chosen as $\rho = \rho_0 = 1$. The initial flow field is static. The numerical results are obtained after running 20 periods. In Fig. 3, the velocity profile across two plates at specific times are drawn in contrast with the analytical solutions. It can be found that numerical results agree with the analytical solutions very well with the unsteady force field.

C. Compressible thermal Poiseuille flow

The third numerical benchmark is the compressible thermal Poiseuille flow. In this numerical case, the flow is bounded by two parallel plates, of which the temperature of the bottom plate is $\theta_b = 1.0$ and the top is $\theta_t = \theta_b + \delta\theta$. The normalized temperature in the flow field is defined as $\theta' = (\theta - \theta_b)/\delta\theta$. ρ_0 is the reference density; H is the height of the channel. The flow is driven by the constant force field (g_x, g_y)

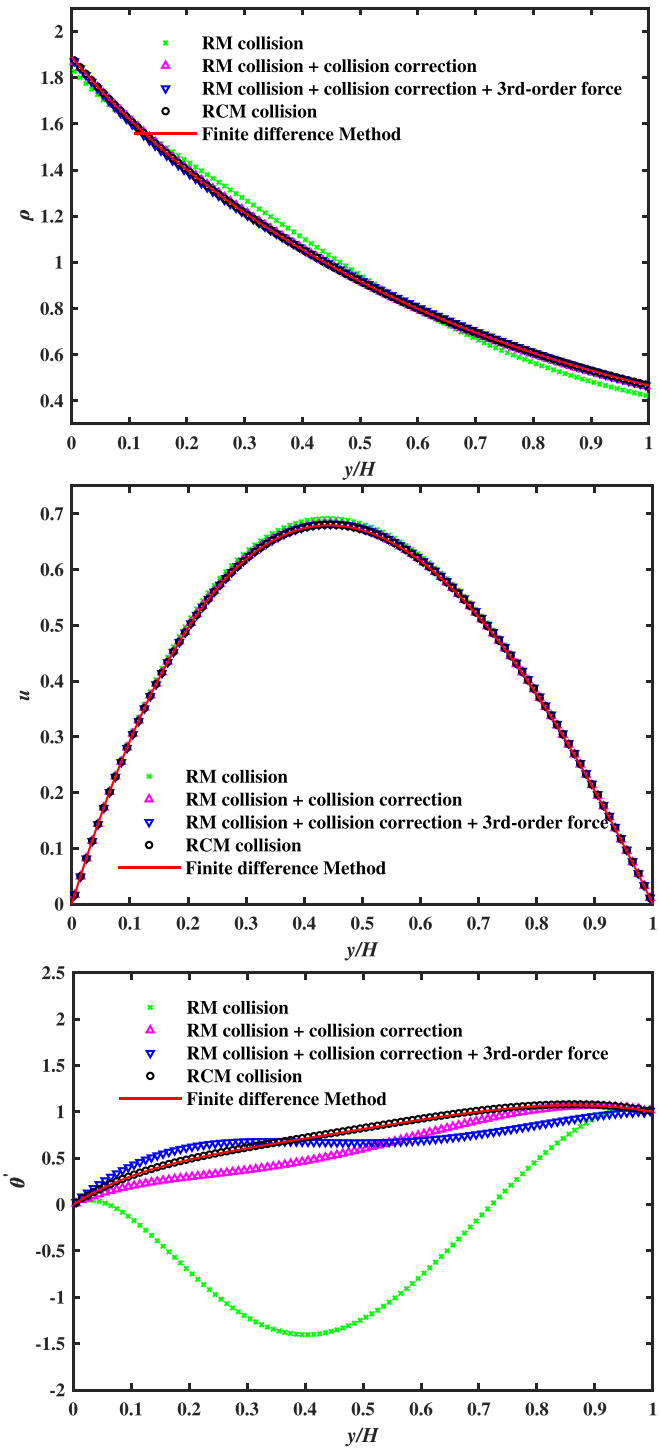

FIG. 4. In the Pr = 0.2 case, the effects of different terms in the third-order relaxation, Eq. (50d), are investigated. "RM collision" denotes only the relaxation of the nonequilibrium RM is retained; "RM collision + collision correction" denotes that the Galilean invariance is considered with the collision correction term; "RM collision + collision correction + 3rd-order force" denotes the third-order force is considered; "RCM collision" denotes the complete collision form with the force correction term.

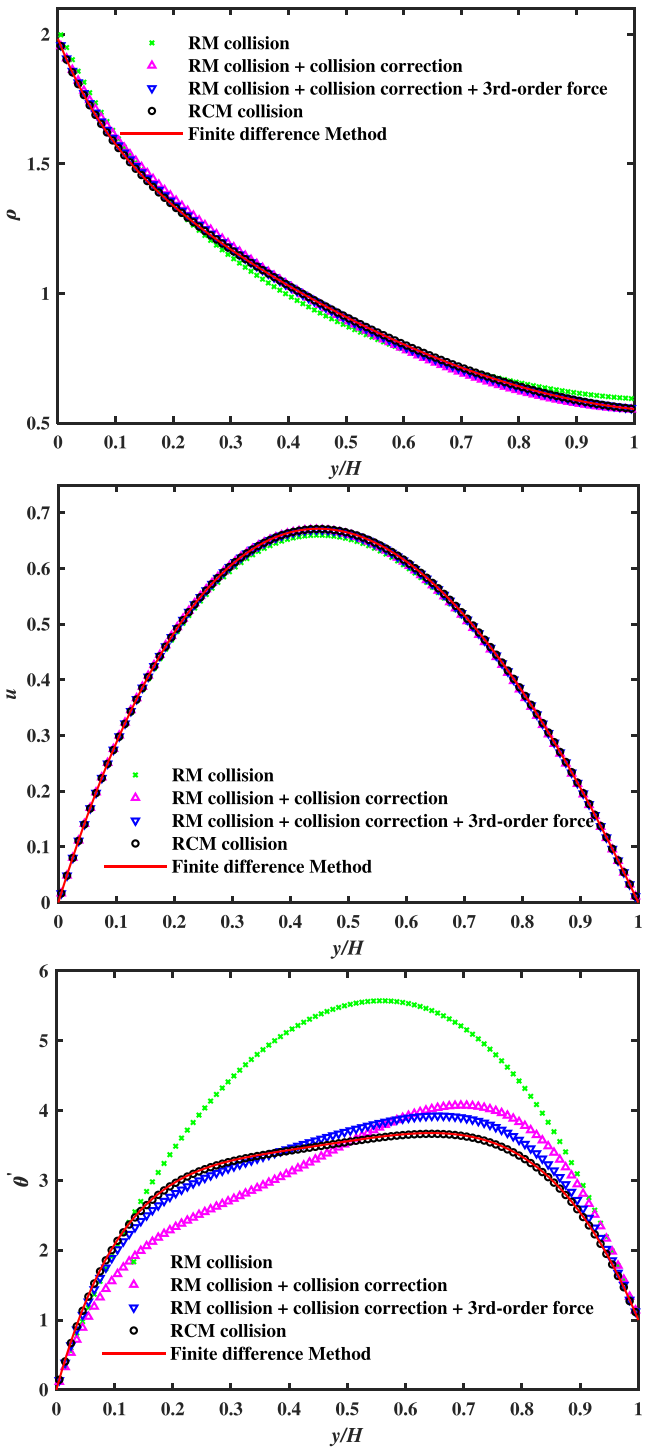

FIG. 5. In the Pr = 2 case, the effects of different terms in the third-order relaxation, Eq. (50d), are investigated. "RM collision" denotes only the relaxation of the nonequilibrium RM is retained; "RM collision + collision correction" denotes that the Galilean invariance is considered with the collision correction term; "RM collision + collision correction + 3rd-order force" denotes the third-order force is considered; "RCM collision" denotes the complete collision form with the force correction term.

with the x axis parallel to the plates. The Mach number is defined as $\mathrm{Ma} = \frac{\rho_0 g_x H^2}{8\mu}$. The Reynolds number is defined as $\mathrm{Re} = \frac{\rho_0 MaH}{\mu}$. The Eckert number is defined as $\mathrm{Ec} = \frac{Ma^2}{\delta\theta c_p}$ with $c_p = \frac{D+2}{2}$ the specific heat ratio at constant pressure. Thus, once the Mach number and the ratio of g_x and g_y are given, the force field (g_x, g_y) can be obtained. Once the Eckert number

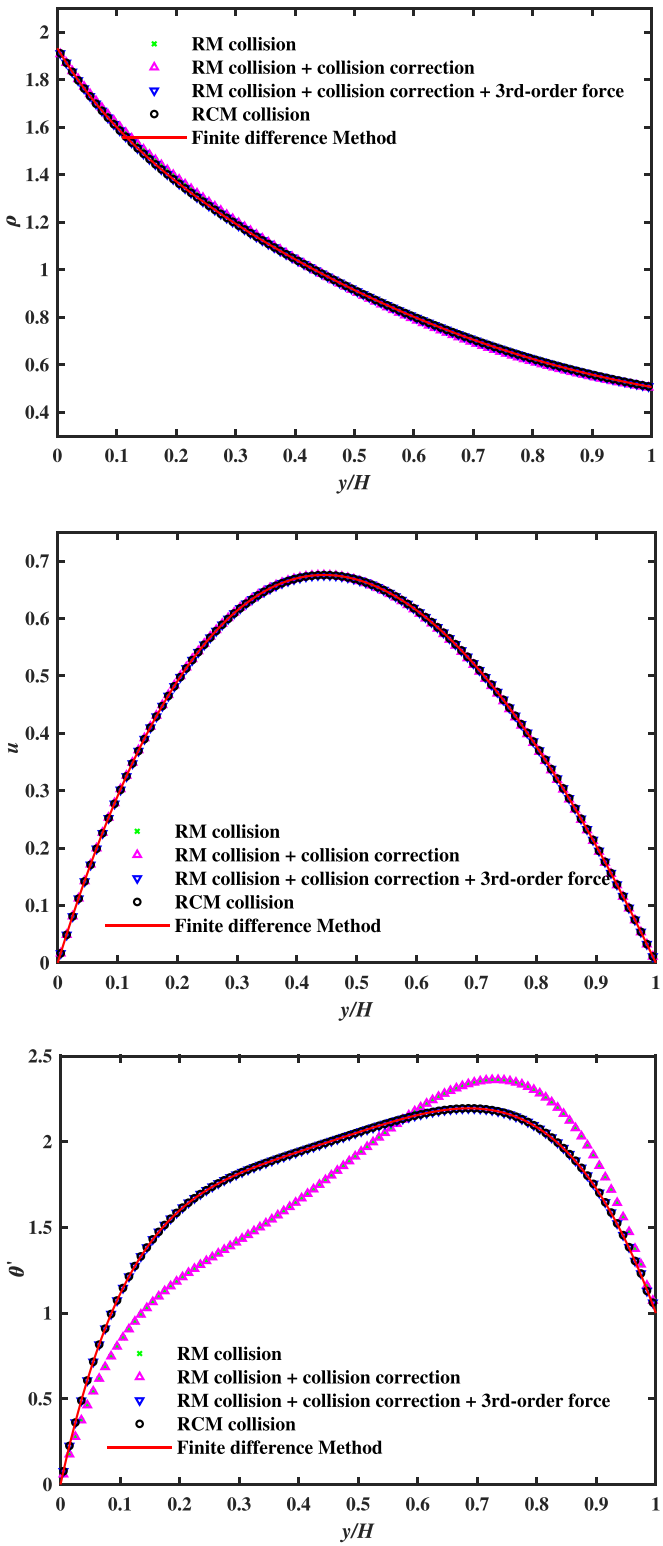

FIG. 6. In the $\mathrm{Pr} = 1$ case, the effects of different terms in the third-order relaxation, Eq. (50d), are investigated. "RM collision" denotes only the relaxation of the nonequilibrium RM is retained; "RM collision + collision correction" denotes that the Galilean invariance is considered with the collision correction term; "RM collision + collision correction + 3rd-order force" denotes the third-order force is considered; "RCM collision" denotes the complete collision form with the force correction term.

is given, the temperature difference between the bottom and top plates will be obtained. The dynamic viscosity μ and $\hat{\tau}_2$ can be determined by the Reynolds number. The thermal conductivity κ and $\hat{\tau}_3$ can be determined by the Prandtl number $\mathrm{Pr} = \frac{\mu c_p}{\kappa} = \frac{\hat{\tau}_2 - 0.5}{\hat{\tau}_3 - 0.5}$. In the present numerical benchmark, the parameters are set as $\mathrm{Ma} = 0.7$, $\mathrm{Re} = 140$, $\mathrm{Ec} = 5$, $g_x/g_y = -50$, $\mathrm{Pr} = 0.2, 1.0, 2.0$, and $H = 100$ lattice. The numerical results with 1000 meshes across the channel simulated by the high-order finite difference method is regarded as the reference results.

To investigate the self-consistence of the present force scheme in the SMRT model, four cases are tested for the third-order relaxation: (1) case 1: the collision form is $(1 - \frac{1}{\hat{\tau}_3})\bar{\boldsymbol{a}}_1^{(3)}$, which is denoted as "RM collision"; (2) case 2: the collision form is $(1 - \frac{1}{\hat{\tau}_3})\bar{\boldsymbol{a}}_1^{(3)} + (\frac{1}{\hat{\tau}_3} - \frac{1}{\hat{\tau}_2})3\boldsymbol{u}\bar{\boldsymbol{a}}_1^{(2)}$, which is denoted as "RM collision + collision correction"; (3) case 3: the collision form is $(1 - \frac{1}{\hat{\tau}_3})\bar{\boldsymbol{a}}_1^{(3)} + (\frac{1}{\hat{\tau}_3} - \frac{1}{\hat{\tau}_2})3\boldsymbol{u}\bar{\boldsymbol{a}}_1^{(2)} + (1 - \frac{1}{2\hat{\tau}_3})\boldsymbol{a}_F^{(3)}$, which is denoted as "RM collision + collision correction + 3rd-order force"; (4) case 4: the collision form is the full expression of Eq. (50d), including the force correction term, which is denoted as "RCM collision."

From Fig. 4 and Fig. 5, it can be found that the results of the proposed "RCM collision" agree well with the reference, while the normalized temperature of other cases, especially the "RM collision" case, deviate the reference remarkably. Each term of the third-order collision correction term, third-order force term, and force correction term plays a significant role in accurate simulation of the density, velocity, and temperature field for the flows of the nonunit Prandtl number. From Fig. 6, it can be found that the results of the proposed "RCM collision" also agree well with the reference data. Due to the unit Prandtl number, the collision forms of case (1) and case (2) are identical for the vanishing collision correction term, while the collision forms of case (3) and case (4) are identical for the vanishing force correction term. In general, it can be found that the numerical simulation results match the theoretical formulas very well.

IV. CONCLUSIONS AND DISCUSSIONS

In the present work, the force scheme for the lattice Boltzmann method based on kinetic theoretical formulation is proposed for the SMRT collision model. The proposed SMRT collision model with force term is identical to the collision model with force term in the RM space if and only if all the relaxation rates are equal to each other. The cross-talk effect between the force terms in the collisions of third order and higher are completely removed in the present model. The proposed force scheme for the SMRT collision model is numerically verified for isothermal flow and thermal flow with arbitrary Prandtl number. It should be stressed that the present force scheme is the first strict and complete one for the single particle distribution function lattice Boltzmann model which is capable of Navier-Stokes-Fourier equations. This generic approach of incorporating the force scheme actually can be applied to a wide range of collision models.

ACKNOWLEDGMENTS

This work was supported by the National Natural Science Foundation of China Grants No. 51979053 and No.

92152107, the Natural Science Foundation of Heilongjiang Province Grant No. LH2021A007, Heilongjiang Touyan Innovation Team Program No. TY2010010601, Department of Science and Technology of Guangdong Province Grants No. 2019B21203001 and No. 2020B1212030001, and Shenzhen Science and Technology Program Grant No. KQTD20180411143441009.

APPENDIX: MRT FORCE SCHEME IN HERMITE RAW-MOMENT SPACE

In the Hermite raw-moment MRT model, the Galilean invariance and rotational invariance are not considered. For the convenient reading of this manuscript, the derivation of the force scheme of the Hermite raw-moment MRT model is stated here. Similarly, starting from Eq. (19), we can get the same evolution equation as Eq. (24) for the MRT model in the Hermite raw-moment space. The transform of the right-hand side of Eq. (24) to the Hermite RM space is

$$\bar{\boldsymbol{a}}_p^{(n)} = \bar{\boldsymbol{a}}^{(n)} - \frac{1}{\tau_n}\left(\boldsymbol{a}^{(n)} - \boldsymbol{a}_0^{(n)}\right) + \boldsymbol{a}_F^{(n)}, \tag{A1}$$

in which the subscript p denotes the postcollision state and $\bar{\boldsymbol{a}}^{(n)}$ is the mapping of Eq. (23) in Hermite RM space

$$\bar{\boldsymbol{a}}^{(n)} = \boldsymbol{a}^{(n)} + \frac{1}{2\tau_n}\left(\boldsymbol{a}^{(n)} - \boldsymbol{a}_0^{(n)}\right) - \frac{1}{2}\boldsymbol{a}_F^{(n)}. \tag{A2}$$

Using the above equation, Eq. (A1) can be written as the following explicit and simple moment collision equation:

$$\bar{\boldsymbol{a}}_p^{(n)} = \boldsymbol{a}_0^{(n)} + \left(1 - \frac{1}{\hat{\tau}_n}\right)\bar{\boldsymbol{a}}_1^{(n)} + \left(1 - \frac{1}{2\hat{\tau}_n}\right)\boldsymbol{a}_F^{(n)}, \quad n \geqslant 1, \tag{A3}$$

in which $\hat{\tau}_n = \tau_n + \frac{1}{2}$, $\bar{\boldsymbol{a}}_1^{(n)} = \bar{\boldsymbol{a}}^{(n)} - \boldsymbol{a}_0^{(n)}$, and $\bar{\boldsymbol{a}}_p^{(0)} = \boldsymbol{a}_0^{(0)}$.

In the numerical implementation, $\boldsymbol{a}_F^{(n)} = n\boldsymbol{g}\boldsymbol{a}^{(n-1)}$. If the nonequilibrium contributions beyond second order are ignored, we have

$$\boldsymbol{a}_F^{(1)} = \rho\boldsymbol{g}, \tag{A4a}$$

$$\boldsymbol{a}_F^{(2)} = 2\rho\boldsymbol{g}\left(\boldsymbol{u} - \frac{\boldsymbol{g}}{2}\right), \tag{A4b}$$

$$\boldsymbol{a}_F^{(3)} = 3\rho\boldsymbol{g}[\boldsymbol{u}\boldsymbol{u} + (\theta - 1)\boldsymbol{\delta}], \tag{A4c}$$

$$\boldsymbol{a}_F^{(4)} = 4\rho\boldsymbol{g}[\boldsymbol{u}\boldsymbol{u}\boldsymbol{u} + 3(\theta - 1)\boldsymbol{u}\boldsymbol{\delta}]. \tag{A4d}$$

In the Hermite RM collision operator, $\bar{\boldsymbol{a}}_1^{(1)} = -0.5\rho\boldsymbol{g}$, which is indicated by Eq. (29). $\bar{\boldsymbol{a}}_1^{(n)}$ $(n = 2, 3)$ is obtained by the projection method. The fourth order term can be obtained by the projection method or the recursive approach as $\bar{\boldsymbol{a}}_1^{(4)} = 4\boldsymbol{u}\bar{\boldsymbol{a}}_1^{(3)} - 6\boldsymbol{u}_1\bar{\boldsymbol{a}}_1^{(2)} + 4(\boldsymbol{u}\boldsymbol{u}_2)\bar{\boldsymbol{a}}_1^{(1)}$. Thus the postcollision particle distribution function can be evaluated as

$$\bar{f}_{i,p} = \omega_i \sum_{n=0}^{4} \frac{1}{n!}\bar{\boldsymbol{a}}_p^{(n)} : \mathscr{H}^{(n)}(\boldsymbol{\xi}_i). \tag{A5}$$

Then the stream can be conducted as

$$f_i(\boldsymbol{x} + \boldsymbol{\xi}_i, t + 1) = \bar{f}_{i,p}(\boldsymbol{x}, t). \tag{A6}$$

[1] S. A. Bawazeer, S. S. Baakeem, and A. A. Mohamad, Arch. Comput. Methods Eng. **28**, 4405 (2021).
[2] P. L. Bhatnagar, E. P. Gross, and M. Krook, Phys. Rev. **94**, 511 (1954).
[3] X. Shan and H. Chen, Phys. Rev. E **47**, 1815 (1993).
[4] X. Shan and H. Chen, Phys. Rev. E **49**, 2941 (1994).
[5] H. Huang, M. Krafczyk, and X. Lu, Phys. Rev. E **84**, 046710 (2011).
[6] K. Sun, T. Wang, M. Jia, and G. Xiao, Physica A **391**, 3895 (2012).
[7] Z. Guo, C. Zheng, and B. Shi, Phys. Rev. E **65**, 046308 (2002).
[8] Z. Yu and L.-S. Fan, J. Comput. Phys. **228**, 6456 (2009).
[9] Q. Li, K. H. Luo, and X. J. Li, Phys. Rev. E **86**, 016709 (2012).
[10] A. L. Kupershtokh, in *Proceedings of the 5th International EDH Workshop* (Université de Poitiers, Poitiers, 2004), pp. 241–246.
[11] D. Lycett-Brown and K. H. Luo, Phys. Rev. E **94**, 053313 (2016).
[12] A. De Rosis, Phys. Rev. E **95**, 023311 (2017).
[13] L. Fei and K. H. Luo, Phys. Rev. E **96**, 053307 (2017).
[14] X. Shan and X. He, Phys. Rev. Lett. **80**, 65 (1998).
[15] X. Shan, X.-F. Yuan, and H. Chen, J. Fluid Mech. **550**, 413 (2006).
[16] N. S. Martys, X. Shan, and H. Chen, Phys. Rev. E **58**, 6855 (1998).
[17] X. He, S. Chen, and G. D. Doolen, J. Comput. Phys. **146**, 282 (1998).
[18] X. Shan, Phys. Rev. E **100**, 043308 (2019).
[19] X. Li, Y. Shi, and X. Shan, Phys. Rev. E **100**, 013301 (2019).
[20] X. Shan, X. Li, and Y. Shi, Philos. Trans. R. Soc. A **379**, 20200406 (2021).
[21] X. Li and X. Shan, Phys. Rev. E **103**, 043309 (2021).
[22] Y. Shi and X. Shan, Phys. Fluids **33**, 037134 (2021).
[23] S. Chapman and T. G. Cowling, *The Mathematical Theory of Non-uniform Gases*, 3rd ed. (Cambridge University Press, Cambridge, UK, 1970).
[24] K. Huang, *Statistical Mechanics*, 2nd ed. (John Wiley & Sons, New York, 1987).
[25] H. Grad, Commun. Pure Appl. Math. **2**, 325 (1949).
[26] H. Grad, Commun. Pure Appl. Math. **2**, 331 (1949).
[27] O. P. Malaspinas, Lattice Boltzmann method for the simulation of viscoelastic fluid flows, Ph.D. thesis, École Polytechnique Fédérale de Lausanne, 2009.
[28] X. Li, X. Shan, and W. Duan, Acta Aerodyn. Sin. **40**, 46 (2022).
[29] J. Meng and Y. Zhang, J. Comput. Phys. **258**, 601 (2014).